RESEARCH PAPER



Decoding Fine API Agglomeration as a Key Indicator of Powder Flowability and Dissolution: Impact of Particle Engineering

Sangah Kim¹ · Mirna Cheikhali¹ · Rajesh N. Davé¹

Received: 28 March 2022 / Accepted: 11 May 2022 © The Author(s), under exclusive licence to Springer Science+Business Media, LLC, part of Springer Nature 2022

Abstract

Purpose Fine API agglomeration and its mitigation *via* particle engineering, i.e., dry coating, remains underexplored. The purpose was to investigate agglomeration before and after dry coating of fine cohesive APIs and impact on powder processability, i.e., flowability (FFC), bulk density (BD), and dissolution of BCS Class II drugs.

Method Ibuprofen (three sizes), fenofibrate, and griseofulvin (5–20 μ m), before and after dry coating with varying amounts of hydrophobic (R972P) or hydrophilic (A200) nano- silica, were assessed for agglomeration, FFC, BD, surface energy, wettability, and dissolution. The granular Bond number (Bo_g), a dimensionless parameter, evaluated through material-sparing particle-scale measures and particle-contact models, was used to express relative powder cohesion.

Results Significant powder processability improvements after dry coating were observed: FFC increased by multiple flow regimes, BD increased by 25–100%, agglomerate ratio (AR) reduction by over an order of magnitude, and greatly enhanced API dissolution rate even with hydrophobic (R972P) silica coating. Scrutiny of particle-contact models revealed non-triviality in estimating API surface roughness, which was managed through the assessment of measured bulk properties. A power-law correlation was identified between AR and Bo_g and subsequently, between AR and FFC & bulk density; AR below 5 ensured improved processability and dissolution.

Conclusion Agglomeration, an overlooked material-sparing measure for powder cohesiveness, was a key indicator of powder processability and dissolution. The significant agglomerate reduction was possible *via* dry coating with either silica type at adequate surface area coverage. Reduced agglomeration after dry coating also countered the adverse impact of increased surface hydrophobicity on dissolution.

KEY WORDS dry coating · granular bond number · powder agglomeration · powder processability · powder roughness

INTRODUCTION

Increased use of fine active pharmaceutical ingredients (API) powders stems from the poor solubility of the majority of the drugs already marketed or under development (1,2), which requires milling to increase the available surface area (3–7). Unfortunately, milling leads to high level of cohesion due to increased interparticle adhesion force, typically arising from van der Waals (vdW) attraction, in relation to individual particle's weight (8–11). This adversely impacts bulk powder properties and hence their processability (12–15). As a result of their finer size leading to increased cohesion, fine

API powders flow and pack poorly, and form large agglomerates (4,12,16,17). Agglomeration delays their dissolution rate, effectively negating the intent of size reduction (4,18). In addition, agglomeration unfavorably impacts API blend uniformity (19,20).

Dry coating is an emerging approach to counter cohesiveness of fine APIs and ensuing poor processability, which collectively represents poor flowability, low packing density, excessive agglomeration, and inadequate dissolution rates (13,14,16,17,21,22). In 6, a solvent-free method, fine cohesive powders (host particles) and nano-additives (guest particles) are mixed at high intensity to uniformly distribute the nano guest particles onto the host particles, creating nano-scale surface roughness (13,14). As analyzed through the proposed particle-contact models (13,14), the interparticle adhesion force is reduced by over an order of magnitude due to dry coating, generally in proportion to the size ratio of

Published online: 14 June 2022



Rajesh N. Davé dave@njit.edu

New Jersey Center for Engineered Particulates, New Jersey Institute of Technology, Newark, New Jersey 07102, USA

the API (host) and guest (nano silica); more so than altered surface energy after coating. As a result, dry coated cohesive particles have been reported to show improved bulk properties, such as enhanced flowability, bulk density, and reduced agglomeration, leading to faster dissolution rates and blend uniformity (16,19–24).

The rather underexplored topic of reduced agglomeration and its subsequent impact on powder processability and dissolution after the dry coating has been a subject of recent investigations (22). It was shown that agglomeration reduction through dry coating could counter the adverse impact of increased hydrophobicity even if the coating material such as R972P, hydrophobic silica, was used, leading to improved dissolution rates (22). In that work, deionized water was used for dissolution testing to better discern the impact of surface hydrophobicity and the combined effect of the drug particle surface hydrophobicity and agglomerate size could explain the dissolution behavior of fine ibuprofen ($\sim 10~\mu m$) (22). A question remains, however, that if the hydrophobic silica could result in an increased dissolution rate if a more hydrophobic drug or much finer API size was considered.

The effective cohesion of finer drug powders could be captured by a dimensionless force parameter called the granular Bond number (Bo_{o}) , which is the ratio of cohesive (vdW) and gravitational forces (8,12,13,25-27). Generally, when $Bo_{g} < 1$, particles are non-cohesive and do not agglomerate, whereas for $Bo_g > 1$, which is the case for fine API powders, they are cohesive and agglomerate. The advantage of using Bo_{σ} as a scaling parameter is that it could account for variations in particle properties other than the size such as their surface energy, surface roughness, etc., hence it is highly applicable to powder materials before and after dry coating (15,28). Estimation of Bo_g , which requires the calculation of the cohesion force (typically the van der Waals (vdW) attraction), is relatively easy for smooth spherical powders. Unfortunately, most powders are naturally rough and are non-spherical. For rough powders, classical contact models are available (13,29,30). However, these are single asperity models that cannot account for the distribution of surface roughness which involves multi-asperity contacts for which improved models have been proposed (14,31). Using the most relevant multi-asperity model (14) requires measuring surface energy of each powder, particle size, and ensuring that the powders do not greatly deviate from standard assumptions including estimated asperity size, uniform asperity distribution, and spherical shapes, since those could limit its applicability (15,28). Notwithstanding the effort involved in estimating Bo_g , its advantages have been shown in scaling agglomeration (12), the minimum bubbling velocity in fluidization (27), flowability (32), and packing or bulk density (15,26,28). Prevalence of such correlations between various bulk properties that are all significantly impacted by cohesion, suggests that any one of those properties could be used to estimate the degree of powder cohesion before and after dry coating without the need to explicitly estimate Bo_g . Consequently, powder agglomeration was considered as a key early indicator of powder cohesion, hence powder processability, including API dissolution rate, the focus and novelty of this paper. That is also because powder agglomeration could be measured via simple, material sparing imaging techniques, in contrast to the assessment of flowability, packing density, etc. requiring more time and larger amounts of powder (22).

Towards the above-mentioned main objective as well as to further substantiate the importance of fine powder agglomeration over altered surface hydrophobicity after hydrophobic silica coating on the dissolution rate of more hydrophobic or finer APIs, ibuprofen (Ibu; three sizes, 20, 10, and 5 μ m), less soluble fenofibrate (FNB; ~7 μ m), and, griseofulvin (GF; ~9 μm), less hydrophobic than Ibu yet less water-soluble, were selected as model poorly water-soluble BCS Class II drugs. FNB and GF sizes were comparable to finer Ibu. GF was selected because of its different surface morphology, which poses significant challenge in achieving desired performance improvement after dry coating (22,28). First, the affinity between each API and each silica type was evaluated through the measurement of their surface energy. Next, the impact of two different types of silica, hydrophobic R972P and hydrophilic A200, and their varying theoretical surface area coverage (SAC) amounts were investigated for all APIs on powder flowability, BD, agglomeration, surface energetics, and wettability. The Bo_g values for all uncoated and dry coated APIs were computed using their surface energy values as well as the particle contact-models requiring particle-scale measures such as particle density, particle size, and surface roughness values. The bulk measures such as the agglomeration, BD, and flow function coefficient (FFC) were assessed against the Bo_{o} outcomes computed through different surface roughness approximations. Finally, the API dissolution rates were measured using the USP IV apparatus and a sodium dodecyl sulfate (SDS) solution (12 mM), selected due to poor solubility of FNB. All the bulk performance measures including dissolution rates were assessed to test the main hypothesis of using powder agglomeration as a key indicator of powder processability and dissolution.

MATERIALS AND METHOD

Materials

Three BCS class II drugs were selected as the model APIs; fenofibrate (FNB, Ahmedabad, India), ibuprofen (Ibu, gifted from BASF, USA), and griseofulvin (GF, Hegno, China). The as-received Ibu (d_{50} of ~70 μ m) was milled down to



three different finer sizes (d_{50} of ~20, 10, 5 µm). The asreceived FNB (d_{50} of ~30 µm) was milled down to finer size as well (d_{50} of ~ 10 µm). As-received GF was ~ 10 µm, hence no further micronization was necessary. Aerosil 200 (nano-sized hydrophilic fumed silica) and R972P (nanosized hydrophobic fumed silica), both donated by Evonik Corporation (Piscataway, NJ, USA), were selected as coating materials (22). Sodium dodecyl sulfate (SDS, Sigma-Aldrich, USA), was used to prepare 12 mM of SDS aqueous solution as a biorelevant dissolution medium since the solubility of FNB was undetectable in de-ionized water (33). The concentration of 12 mM SDS allowed the FNB detection by allowing it to dissolve while still ensuring enough discernment between the dry coating formulations for all the APIs selected. The details of the selected APIs are listed in Table I, including their log P values and solubilities in 12 mM of SDS aqueous solution, the dissolution and wetting medium in which the dissolution rate and liquid penetration rates were measured.

Method

Preparation of API by Milling

Three different Ibu and FNB were prepared by milling with a fluidized energy mill (FEM) (Pharmaceutical Micronizer Fluidized Energy Grinding Jet mill, Sturtevant Inc., Hanover, Massachusetts). The feeding rate, feeding pressure, and grinding pressure, three parameters that control the milled size (4), were selected by trial and error, see the *Supplementary Materials* in Table S1. The details of the parameters and operation methods may be found elsewhere (4).

Dry Coating

A high-intensity vibratory mixer (LabRAM, Resodyn, USA), which serves as a material sparing benchmarking device, was used as per previously discussed protocols to dry coat the APIs (22). The amount of silica was normalized by the API particle size *via* estimating the theoretical SAC,

see Eq. (1), which assumes uniform particle sizes and silica distribution (13).

Weight percent of silica required (%) =
$$\frac{\text{SAC}d_0^3 \rho_d}{D_0^3 \rho_D} \frac{4D_0^2}{d_0^2} \times 100$$
(1)

 D_0 and d_0 are the d_{50} of the host particle (API) and the guest particle (fumed nano-silica), respectively, while ρ_D and ρ_d are the densities of the host and guest particles, respectively. The dry coating formulations and corresponding SAC values as per Eq. (1) for all APIs are shown in Table II. It is noted that the actual SAC values may differ due to the coating effectiveness that differs for each API and because the API particles are non-spherical and have polydisperse size distributions. While the evaluation of actual SAC could be useful, for the present work, it is mainly used to understand the relative impact of the silica amounts.

SEM Imaging

The surfaces of uncoated and dry coated APIs were analyzed under a Scanning Electron Microscopy (SEM, EM JSM-7900F, JEOL) for qualitative assessment of dry coating effectiveness. The sample preparation method is discussed in detail elsewhere (22).

Primary and Agglomerate Size Evaluations

The primary particle size distribution was measured *via* compressed dry air dispersion (1 bar dispersion, selected based on pressure titration) using a laser diffraction particle sizer (Rodos/Helos, Sympatec, USA). Gentler, gravity dispersion was used for a more reliable measure of agglomerate particle size distribution through Gradis dynamic imaging particle sizer system (Gradis/QicPic, Sympatec, USA). The strength of these particle sizers is in their reliable and repeatable measurement, which is accompanied by a minimal particle sample requirement. One measurement required less than ~3 g sample for replicate measurements to ensure

Table I Properties of the APIs Considered in this Investigation

API	Particle density (g/mL)	Prior to the dry coating (Preparation)	Log P (Azad <i>et al.</i> 2016; kim <i>et al.</i> 2021)	Solubility in 12 mM SDS solution at the ambient condition (mg/L)	Melting Point at 1 atm (°C) (Azad et al. 2016; kim et al. 2021)
Ibuprofen20	1.05 ± 0.01	Fluidized energy milled	3.9	$550 \pm 2 \text{ mg}$	75–77
Ibuprofen10	1.07 ± 0.01				
Ibuprofen5	1.07 ± 0.02				
Fenofibrate	1.25 ± 0.01	Fluidized energy milled	5.24	$38 \pm 1 \text{ mg}$	79–82
Grise of ulvin	1.51 ± 0.02	As Received	2.18	$365 \pm 2 \text{ mg}$	220



Table II Silica weight % for dry coating at all SAC levels for R972P and A200 silicas for the APIs

		Weight perc	ent (%)	Weight percent (%)		
	SAC%	R972P	API	A200	API	
Ibu20	25	0.58	99.42	0.28	99.72	
	50	1.15	98.85	0.55	99.45	
	75	1.73	98.27	0.83	99.17	
	100	2.30	97.70	1.10	98.90	
Ibu10	25	0.92	99.08	0.52	99.48	
	50	1.84	98.16	1.03	98.97	
	75	2.76	97.24	1.55	98.45	
	100	3.68	96.32	2.07	97.93	
Ibu5	25	1.22	98.78	0.69	99.31	
	50	2.44	97.56	1.38	98.62	
	75	3.66	96.34	2.07	97.93	
	100	4.88	95.12	2.76	97.24	
FNB	25	1.00	99.00	0.56	99.44	
	50	2.00	98.00	1.13	98.87	
	75	3.00	97.00	1.69	98.31	
	100	4.00	96.00	2.25	97.75	
GF	25	0.57	99.43	0.32	99.68	
	50	1.14	98.86	0.64	99.36	
	75	1.72	98.28	0.96	99.04	
	100	2.29	97.71	1.28	98.72	

repeatability. The details of these instruments and their usage may be found elsewhere (22).

Bulk Powder Properties: Bulk Density and Flowability (FT4)

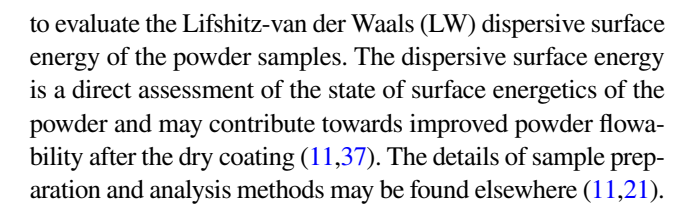
FT4 (Freeman Technology, UK) was employed for the bulk powder properties analysis considering the small sample size required (10 mL to 25 mL) and the ability to condition and initialize the powders for repeatable measurements. FT4 measures both the major principal stress (MPS) and unconfined yield strength (UYS), where the ratio between MPS and UYS gives the flow function coefficient, FFC (34,35). Following Schulze scale, measured FFC can be used to discern the flow regime where the tested powders belong. Details of measurement methods maybe found elsewhere (19,22,36).

Particle (True) Density Measurement

True particle density measurements employed a Multipycnometer (P/N 02,029–1, Quantachrome Instruments, USA). For each case, five to ten repeated measurements were taken under a helium environment to ensure repeatability.

Surface Energy Measurement

An automated inverse gas chromatography (SEA-IGC; Surface Energy Measurement Systems Ltd., UK) was employed



Evaluation of Host-Guest Compatibility

The compatibility of the guest particle (coating material) and the host particle (API) can be predicted based on the spreading coefficient calculation of material B on material A as shown in Eq. (2) and the corresponding *coating quality index*, CQ_n in Eq. (3) (38).

Spreading coefficient of material Bon A,^{B/A}
$$\lambda = 4 \left[\frac{{}^{A}\gamma_{d}^{B}\gamma_{d}}{{}^{A}\gamma_{d} + {}^{B}\gamma_{d}} + \frac{{}^{A}\gamma_{p}^{B}\gamma_{p}}{{}^{A}\gamma_{p} + {}^{B}\gamma_{p}} - \frac{{}^{B}\gamma_{d}^{B}\gamma_{d}}{2} \right]$$
(2)

$$Q_i = |^{B/A} \lambda - A/B \lambda| \tag{3}$$

In the above, ${}^A\gamma_d$ and ${}^B\gamma_d$ are the dispersive components, whereas ${}^A\gamma_p$ and ${}^B\gamma_p$ are the Lewis acid–base components of the surface energy of two materials, respectively. The difference in the spreading coefficient, which is expressed as $CQ_i = |B/A\lambda| - A/B\lambda|$ (39), indicates the affinity between the material A and B, implicitly accounting for the relative particle sizes and explicitly including the dispersive surface energy and polarity of the particles. Jallo *et al.* (2011) suggested the range of values to predict the coating quality as: coating quality to be



(As received)

~ ,						
Guest (Silica) and host (API)	Dispersive SE (mJ/m2)	Polar SE (mJ/m2)	$CQ_i = B/A \lambda - A/B \lambda$ For R972P	Expected R972P coating quality	$CQ_{i} = ^{B/A} \lambda - {}^{A/B} \lambda $ For A200	Expected A200 coating quality
R972P	37.7	5.1	-	-	-	-
A200	48.7	4.7	-	-	-	-
Ibu20	50.1	5.9	26.4	Very good	5.2	Mediocre
Ibu10	47.3	8.1	25.2	Very good	4.0	Poor
Ibu5	83.7	24.6	131.0	Very good	109.8	Very good
FNB (milled)	44.0	6.3	14.8	Very good	6.3	Mediocre
GF	40.5	4.5	4.3	Poor	16.8	Very good

Table III Surface Energy Measurements for All APIs (Hosts) and Nano-Silica (Guests) and Their Compatibility Assessment Through *Coating Quality Index*

very good for $CQ_i > 10$, mediocre (will coat but not as good) for $5 < CQ_i < 10$, and not good for $CQ_i < 5$. The estimate of CQ_i was expected to serve as a preliminary screening tool for selecting suitable guest materials only since it does not account for the mixing process intensity or time as well as ensuing contact forces between the host and guest particles (40).

Wettability Evaluation: Modified Washburn Method

The dissolution process is impacted by the powders surface wettability as well as their agglomerate size, but the outcome is difficult to predict due to their opposing and often confounding effect, especially after the dry coating (22). Here, the modified Washburn method was used to evaluate the surface wettability or the surface wetting angle, which was calculated using Eq. (4) (41–43).

$$m^2 = \left(\frac{C\rho^2\gamma\cos\theta}{\eta}\right)t\tag{4}$$

The above equation was used to estimate the liquid penetration rate through a packed powder bed having geometric packing factor C. Here, m is the mass of liquid penetrated to the packed bed, while ρ , γ , and η , are the density, surface tension, and the viscosity of liquid, respectively. The details regarding the method and sample preparation may be found elsewhere (22,44). Attension Sigma 700 (Biolin Scientific Inc., Linthicum) was used to conduct the liquid penetration test. Before conducting experiments, both the reference and testing liquids were pre-saturated by dissolving the appropriate API minimum of 48 h (22). Considering the small trace amount of SDS in de-ionized water, the density, surface tension, and viscosity of the testing were taken as those of de-ionized water (44).

API Release Rate from Tablets via USP IV Method

An automated flow-through-cell USP IV system (USP IV, SOTAX, Switzerland) coupled with UV-vis

analysis (UV–vis spectrometer, Thermo Scientific, USA) was employed, which ensures the simultaneous wetting of the powders at the onset of the dissolution process (22,45). Following USP < 711 > guidelines, the temperature of the system and the medium flow rate were maintained at 37 \pm 0.2 °C and 16 mL/min, respectively. At a predetermined time-point and detection wavelength, temporal sampling and analysis of the API concentration dissolved were detected. Ibu, FNB, and GF were detected at the wavelength of 222 nm, 291 nm, and 297 nm, respectively.

Before the dissolution test, the solubility or the amount of API required to saturate the 12 mM of SDS aqueous solution was carefully evaluated. Over 3 to 6 h, a supersaturated solution of 12 mM SDS was maintained by gradual additions of 5 to 7 mg of API in 1 L solution. A magnetic stirrer kept the solution stirred at 480 rpm while the temperature was maintained at 25 ± 0.5 °C and measured at intervals using a non-contact handheld IR thermometer (Sigma-Aldrich, USA). Table I shows the experimentally evaluated solubility of each API at the ambient condition in the 12 mM SDS solution, checked against the reported findings for validation (33,46,47).

RESULTS

The compatibility between pairs of host–guest particles (API – nano-silica particles) based on surface energy measurements (see Sect. 2.2.8.1) of both the silica and all the APIs were assessed, see Table III. Estimated values for the R972P coating quality index (CQ_i) using Eq. (3) suggested very good affinities for all the APIs except for GF, for which its CQ_i was below 5. In contrast, for A200, inferior coating quality was predicted for all APIs, except Ibu5 and GF, as CQ_i was below 10 or even 5. A qualitative assessment of the actual coating quality was done through the SEM images; see Fig. 1 for R972P coating and the *Supplementary Materials* Figure S1 for A200 coating. The SEM images indicated that the actual coating quality was better than expected based



on Eq. (3) for many cases. As mentioned before, this could be attributed to the higher intensity of mixing and coating in LabRAM, which could have aided the attachment and spreading of the guest particles onto the surface of host particles (40). Nonetheless, A200 coating for Ibu20, Ibu10, and Ib5, at lower SAC levels such as 25% SAC, was not

as good as that for R972P and exhibited lesser spreading along with a greater tendency for silica particles to aggregate. Consequently, with a possible exception of GF, very good improvements in bulk powder properties were expected from dry coating with R972P, and lesser enhancements from dry coating with A200.

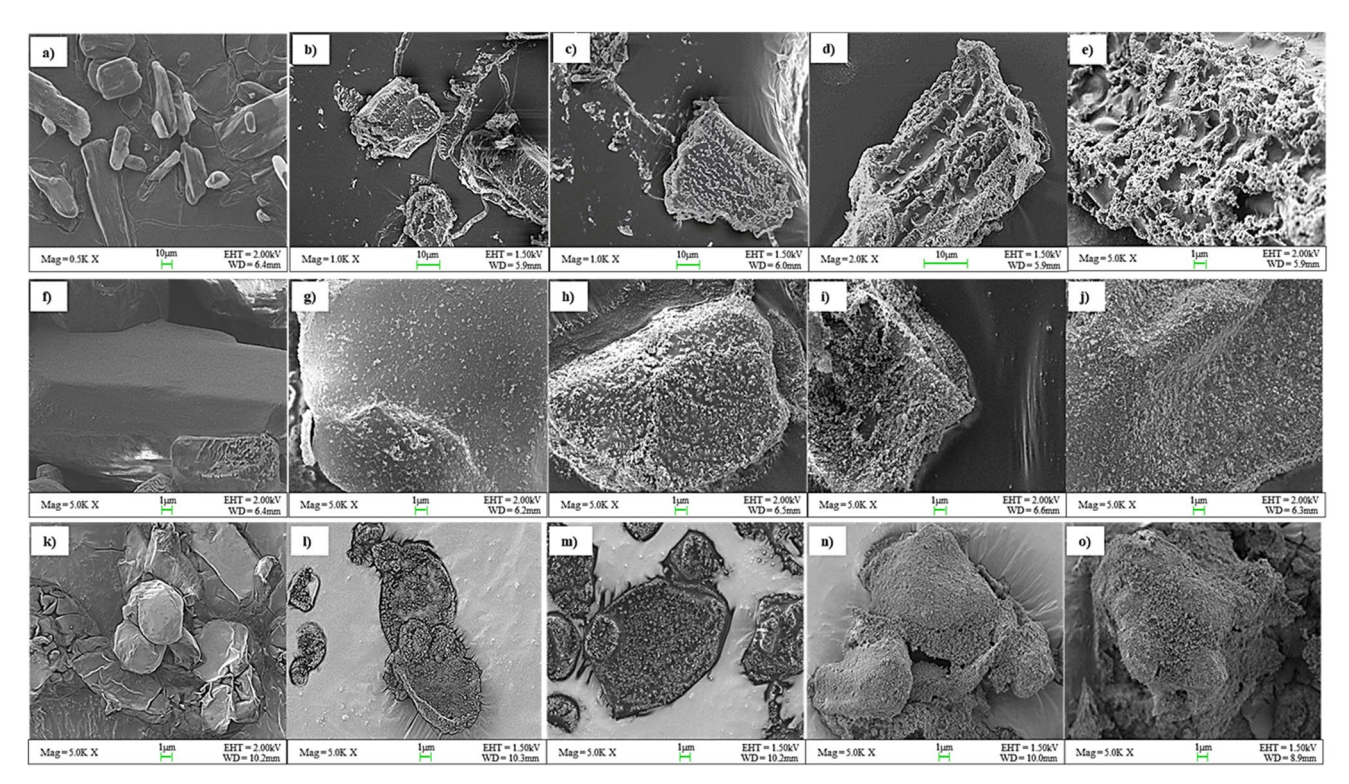


Fig. 1 SEM images of uncoated and R972P coated drug powders. For ibuprofen20 (Ibu20): (a) uncoated, (b) theoretical SAC25%, (c) theoretical SAC50%, (d) theoretical SAC75%, and (e) theoretical SAC100%. For ibuprofen10 (Ibu10): (f) uncoated, (g) theoretical SAC25%, (h) theoretical SAC50%, (i) theoretical SAC75%, and (j) theoretical SAC100%. For ibuprofen5 (Ibu5): (k) uncoated, (l) theoretical SAC25%, (m) theoretical SAC50%, (n) theoretical SAC75%, and (o) theoretical SAC100%. For fenofibrate (FNB): (p) uncoated, (q) theoretical SAC25%, (r) theoretical SAC50%, (s) theoretical SAC75%, and (t) theoretical SAC100%. For griseofulvin (GF): (u) uncoated, (v) theoretical SAC25%, (w) theoretical SAC50%, (x) theoretical SAC75%, and (y) theoretical SAC100%.

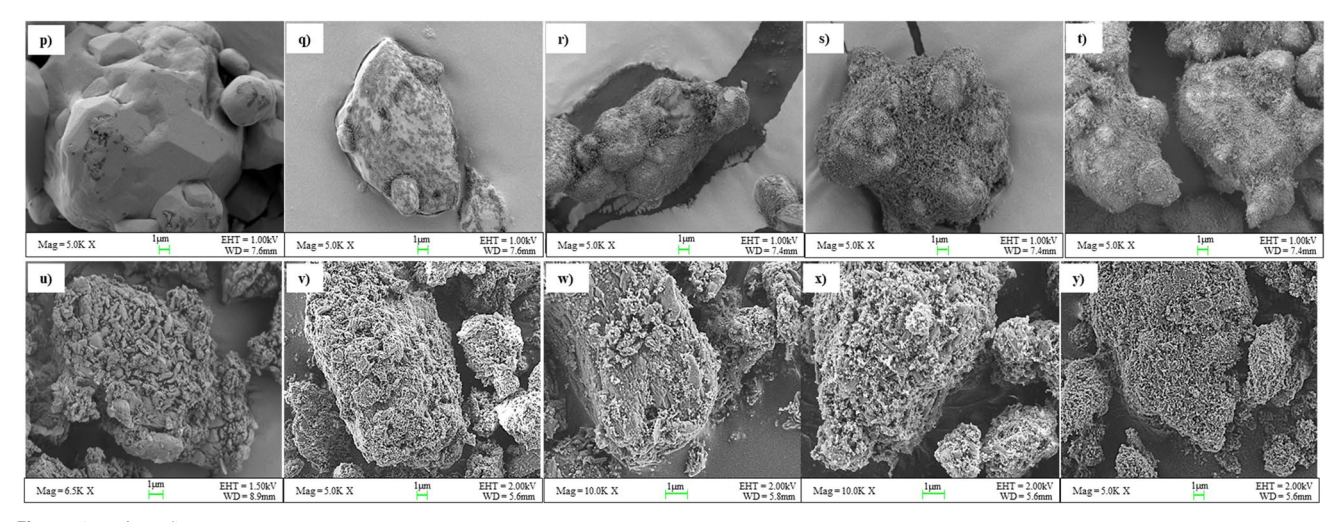


Fig. 1 (continued)



Table IV Nominal API Particle Sizes (d_{50}) Measured Using Rodos/Helos and Gradis/QicPic Before and After Dry Coating and Their Agglomeration Ratios (AR)

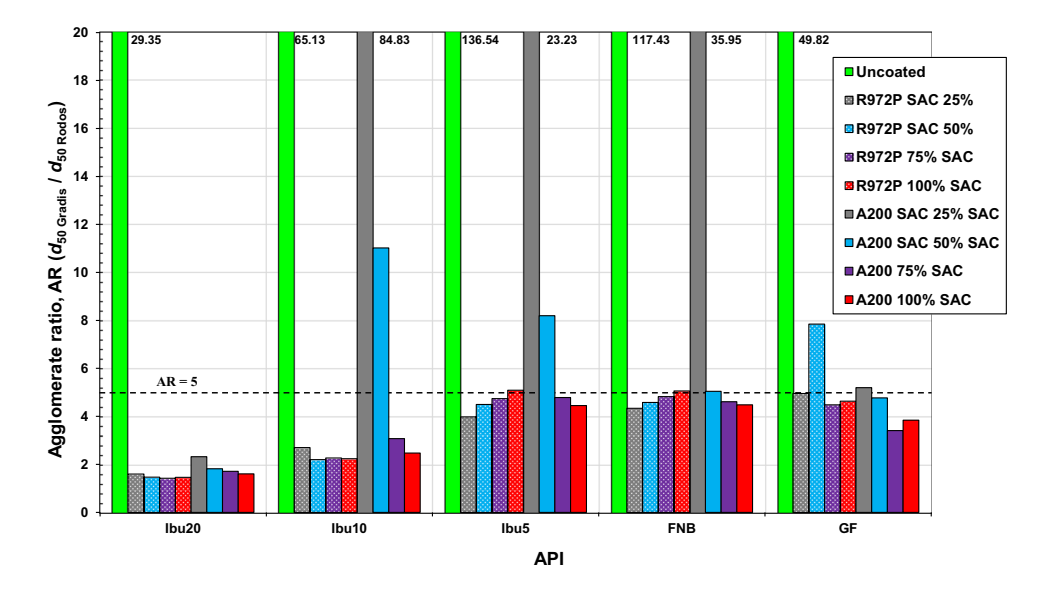
	APIs		Ibu20			Ibu10			Ibu5			FNB			GF	
Coating materials	% SAC	d ₅₀ Rodos (μm)	d ₅₀ Gradis (μm)	AR (d ₅₀ Gradis /d ₅₀ Rodos)	d ₅₀ Rodos (μm)	d ₅₀ Gradis (μm)	AR (d ₅₀ Gradis /d ₅₀ Rodos)		d ₅₀ Gradis (μm)	AR (d ₅₀ Gradis /d ₅₀ Rodos)	d ₅₀ Rodos (μm)	d ₅₀ Gradis (μm)	AR (d ₅₀ Gradis /d ₅₀ Rodos)	d ₅₀ Rodos (μm)		AR (d ₅₀ Gradis /d ₅₀ Rodos)
Uncoated	0	21.6± 0.2	633± 544	29.4	12.6 ± 0.2	818 ± 893	65.1	7.0± 0.3	949±362	136.5	6.9 ± 0.0	808 ± 181	117.4	9.1 ± 0.3	453± 545	49.8
	SAC 25%	21.0 ± 0.2	33.4± 3.3	1.6	10.4 ± 0.1	28.1 ± 3.8	2.7	7.0 ± 0.0	27.7±1.0	4.0	6.1 ± 0.1	26.4 ± 0.8	4.3	8.8 ± 0.4	43.7 ± 4.6	5.0
	SAC 50%	20.8 ±0.1	30.4± 1.8	1.5	10.2 ± 0.1	22.4 ± 0.2	2.2	6.2 ± 0.1	28.0±1.1	4.5	6.0 ± 0.0	27.5 ± 0.7	4.6	8.6 ± 0.1	67.4± 29.2	7.8
R972P	SAC 75%	20.1± 0.3	28.6± 0.6	1.4	10.1 ± 0.0	22.9 ± 0.2	2.3	6.0 ± 0.1	28.3±0.6	4.7	6.2 ± 0.0	29.7 ± 1.2	4.8	8.5 ± 0.3	38.0± 8.8	4.5
	SAC 100%	19.1 ± 0.3	27.8± 0.6	1.5	10.2± 0.0	22.8 ± 0.6	2.2	5.5 ± 0.1	28.1±0.4	5.1	6.4 ± 0.1	32.6 ± 2.2	5.1	8.1 ± 0.2	37.6 ± 13.8	4.6
	SAC 25%	18.8 ± 0.1	43.6± 2.9	2.3	10.3 ± 0.1	877 ± 791	84.8	7.0 ± 0.1	1592±76	23.2	6.2 ± 0.0	221 ± 421	36.0	8.9 ± 0.5	46.4 ± 8.3	5.2
A200	SAC 50%	18.9 ± 0.2	34.4± 1.2	1.9	10.2 ± 0.2	113± 168	11.0	6.7 ± 1.0	55.2±24.5	8.2	6.4 ± 0.0	32.1 ± 6.6	5.0	9.0 ± 0.5	42.7 ± 12.8	4.8
	SAC 75%	18.8 ± 0.2	32.1±1.3	1.7	10.2 ± 0.0	31.4 ± 3.5	3.1	6.7 ± 0.1	31.9±0.8	4.8	6.7 ± 0.0	31.0 ± 1.5	4.6	9.3 ± 0.2	31.6 ± 1.9	3.4
	SAC 100%	19.3 ± 0.2	30.9±1.2	1.6	10.1 ± 0.1	25.1 ± 0.2	2.5	7.1 ± 0.1	31.7±0.7	4.4	6.6 ± 0.0	29.7 ± 3.4	4.5	8.6 ± 0.5	32.9 ± 2.3	3.8

API Agglomeration Before and After Dry Coating

The nominal sizes (d_{50}) for primary and agglomerate particle sizes were measured using the Rodos/Helos and Gradis/QicPic devices to compute agglomerate ratios (AR) in each case before and after dry coating, see Table IV. The dry coating did not change the primary particle sizes assessed using Rodos/Helos at a range of dispersion pressures of very low $(0.1\ \text{bar})$ to high $(1.0\ \text{bar})$; reported at $1.0\ \text{bar})$ but significantly reduced the agglomerate sizes assessed using Gradis/QicPic indicating effective interparticle cohesion reduction

(19,22). That occurred for all 5 APIs, even though there were case-by-case differences, as seen in Fig. 2 and in further detail in Table IV. Typical images of the API agglomerates before and after dry coating, not shown for the sake of brevity, confirmed the overall trend of dramatic reduction in both the agglomerate sizes and their distributions; confirming previously reported limited set of results (19,22). The milling impact on three different milled sizes of Ibu revealed interesting trends as the uncoated milled Ibu powders exhibited increasing surface energy values (Table III), in line with the previous work (11). The corresponding increase in their

Fig. 2 Agglomerate ratio (AR) for each dry coated API powder as a function SAC % and silica type. AR values for all uncoated API powders are capped at 20 (bright green bars) along with the actual numerical values.





effective Hamaker constant, hence particle cohesiveness, was reflected in their increasingly higher agglomerate ratios (AR), ~ 29 , ~ 65 and ~ 137 for Ibu20, Ibu10, and Ibu5 respectively, see Fig. 2. It is noted that all AR values for uncoated powders exceed the capped limit of AR = 20 in Fig. 2, which helps better illustrate the variations in AR after dry coating. The agglomeration for uncoated FNB and GF was also significant, as indicated by AR of ~ 36 and ~ 50 respectively.

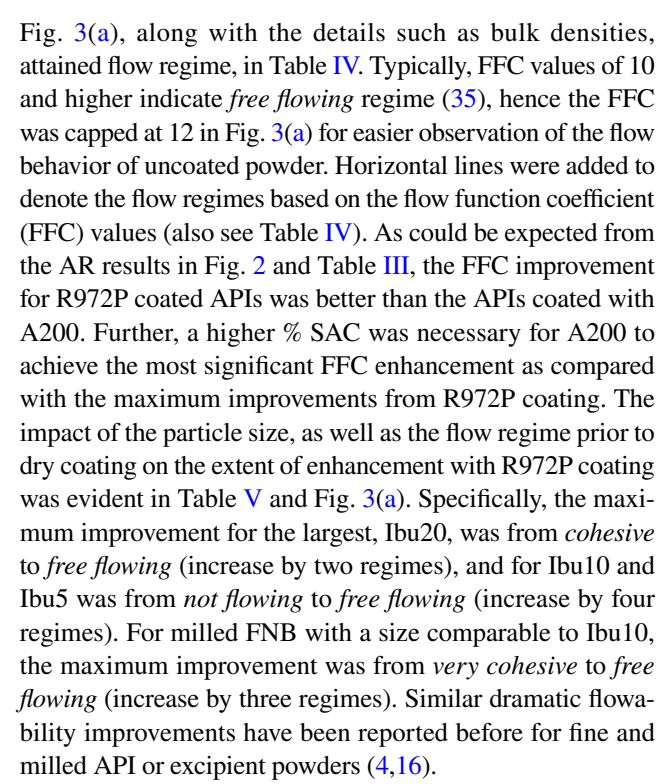
In contrast to uncoated particles, dry coated particles had greatly reduced agglomeration, as seen in AR values, Table IV, more so for R972 coated powders. For three milled Ibu cases, R972P coating led to AR values of less than 2, just above 2, and between 4 and 5 for Iby20, Ibu10, and Ibu5, respectively, representing AR reduction of an order of magnitude or higher. Likewise, for FNB and even GF, which was used as received, the AR values were about 5, which is well over an order of magnitude decrease. The reduction in agglomerate sizes for A200 coated powders was about an order of magnitude, although less than those from R972P coating, expected due to A200's higher total surface energy (see Table III). For finer APIs, i.e., Ibu10, Ibu5, and FNB, 50% or higher SAC of A200 were required to achieve AR reductions comparable to R972P coating.

The impact of the silica SAC was evident from Fig. 2, where for R972P, in general, 25 or 50% SAC was enough. That was in line with the theoretical estimate of about 30–40% SAC being adequate to assure significant cohesion reduction after dry coating based on Chen's multi-asperity model (14). In the case of A200 coating, a higher SAC of about 50% (or higher for Ibu10 and Ibu20) was necessary for the most significant AR reduction, which could be explained based on less effective coating and higher total surface energy of A200 as compared with R972P. Bucking this trend was GF which appeared to have better AR reduction with A200 as compared with R972P at 50% or higher SAC, largely attributed to its better compatibility with A200 (Table II) and surface morphology of GF being drastically different from the other APIs (Fig. 1).

In summary, the agglomeration reduction for all dry coated APIs corroborated with the previously reported flowability enhancements, highlighting that both are strongly driven by a dramatic reduction in cohesion through the dry coating (12–14,32,48). Interestingly, for those dry coated cases for which the AR was 5 or below (noted *via* a dashed line in Fig. 2), the mean particle size of agglomerates ($d_{50 \text{ Gradis}}$) was in a relatively narrow range of 20-40 microns, in line with previously reported settling velocity experiments for weakly cohesive fine powders with surface modification mediated reduced cohesion (12).

Impact of Dry Coating on Flowability and Bulk Density

The dry coating with silica had a profound impact on improved flowability, highlighted through FFC values in

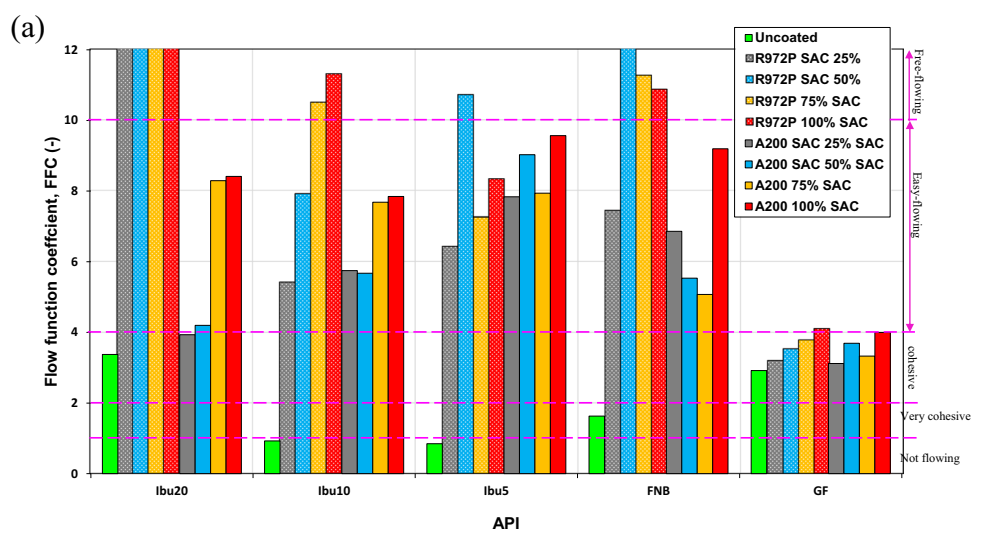


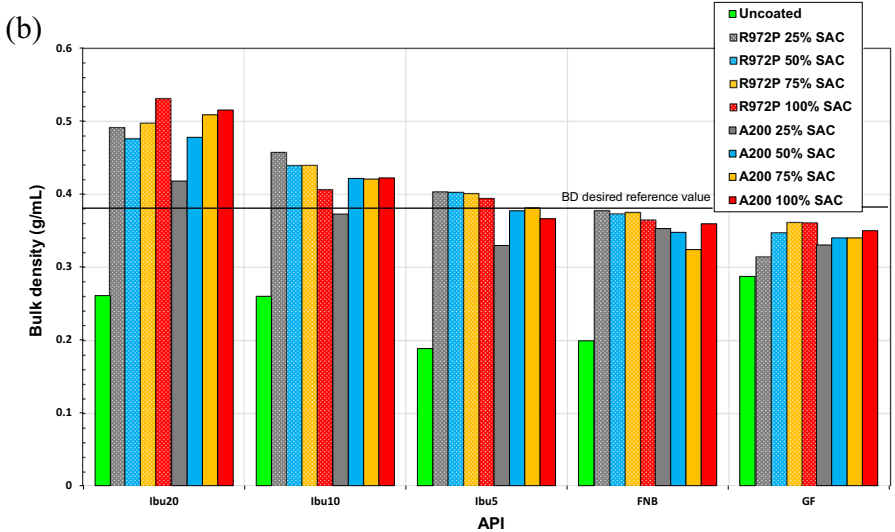
In addition to powder flowability, powder BD influences high-speed direct compressibility of pharmaceutical blends. Bulk densities are plotted in Fig. 3(b) for uncoated and all cases of dry coated APIs. As would be expected, fine APIs powders, including milled versions, have very poor bulk densities, e.g., 0.26 g/mL for Ibu20 and Ibu10, 0.188 g/mL for Ibu5, 0.20 g/mL for FNB, and 0.28 g/mL for GF. After dry coating, the BD significantly improved, see Fig. 3(b). For example, the highest BD level after dry coating for Ibu20 and FNB were twice their uncoated levels thus~100% enhancements and even more for Ibu5. In contrast, BD of GF was only enhanced by~25%.

Overall, in contrast to milled Ibu and FNB, GF failed to achieve appreciable FFC or BD enhancements after dry coating with either silica type. The shift for GF was merely by one flow regime, and that too for the theoretical 100% SAC for either silica type (Table V). Likewise, the BD enhancement was limited to ~25% for R972P silica at 75 or 100% SAC. The need for higher silica amount could be in part due to excessive surface roughness of as received GF, indicated by its higher specific surface area (SSA of 5.04 m²/g) based on BET analysis (28) as compared to milled Ibu 10 (4) (SSA of 2.3 m²/g). Both GF and Ibu10 had about a similar primary particle size, d_{50} of ~ 10 µm, hence nearly double SSA for GF was attributed to its natural macro roughness of ~0.4 μm (Fig. 1). That major morphological difference was the key factor for needing a higher amount of silica. As discussed in the next section on the normalization of powder cohesion and the role of surface roughness, that difference was also responsible for insignificant flowability enhancement after dry coating.



Fig. 3 Bulk powder properties before and after dry coating at varying % SAC for each API. (a) Flowability *via* flow function coefficient, FFC at pre-consolidation of 3 kPa. The dashed lines mark flow regimes. (b) Powder bulk density; horizontal reference line for the desirable BD level for direct compression tableting.





In summary, these results demonstrate remarkable improvements through dry coating in FFC and BD for otherwise very cohesive fine powders that behave like their chemically identical but much larger equivalents. As a side note, for materials with rough surface morphology like GF, higher theoretical % SAC may be necessary to compensate the effect of rough surface morphology that could lead to significant underestimation of the actual SAC. This interesting topic, deemed outside the scope of the current work, would be considered for a future investigation involving several different fine particles having rough morphologies.

Normalization of Cohesion Through Granular Bond Number and Its Relation to AR

As discussed in the introduction, the effective cohesion could be captured by a dimensionless force parameter Bo_g , defined as the ratio of cohesive (vdW) and gravitational forces.

$$Bo_g = \frac{F_{ad}}{F_g} = \frac{F_{vdW}}{\frac{\pi}{6}D^3\rho_p g}$$
 (5)

In Eq. (5), the $F_{\rm ad}$ is the adhesion force, usually the van der Waals force ($F_{\rm vdw}$) for dry fine powders, D is the nominal particle size and ρ_p is the particle material (true) density. Since most pharmaceutical powders are not perfectly smooth and have natural (or induced after dry coating) roughness, the interparticle cohesive force (F_{vdw}) may be estimated using the multi-asperity Chen $et\ al.$ model (14). Accordingly, Eq. (6) accounts for the contact force between two spherical particles with evenly distributed surface asperities. As mentioned above, the asperities arise from either their natural roughness or nano-scale roughness imparted by the uniform coating of silica or similar nano-sized glidant (guest) particles. When the amount of silica particles is not excessive, i.e., the SAC of up to ~30%, the uniform coating of silica leads to predominantly host–guest contacts, and



 Table V
 Bulk Properties of the Powders Before and After the Dry Coating

API	Sample ID	Bulk density (g/mL)	Flow function coefficient, FFC	Flow dynamic	Number of flow regimes improvement after dry coating
Ibu20	uncoated	0.261 ± 0.002	3.38	Cohesive	-
	Ibu20_R972P 25% SAC	0.491 ± 0.026	12.42	Free flowing	2
	Ibu20_R972P 50% SAC	0.476 ± 0.020	15.12	Free flowing	2
	Ibu20_R972P 75% SAC	0.498 ± 0.006	17.31	Free flowing	2
	Ibu20_R972P 100% SAC	0.531 ± 0.007	17.63	Free flowing	2
	Ibu20_A200 25% SAC	0.418 ± 0.005	3.93	Cohesive	0
	Ibu20_A200 50% SAC	0.478 ± 0.016	4.20	Easy flowing	1
	Ibu20_A200 75% SAC	0.509 ± 0.005	8.30	Easy flowing	1
	Ibu20_A200 100% SAC	0.515 ± 0.000	8.42	Easy flowing	1
bu10	uncoated	0.260 ± 0.008	0.93	Not flowing	-
	Ibu10_R972P 25% SAC	0.457 ± 0.008	5.42	Easy flowing	3
	Ibu10_R972P 50% SAC	0.439 ± 0.014	7.91	Easy flowing	3
	Ibu10_R972P 75% SAC	0.440 ± 0.004	10.50	Free flowing	4
	Ibu10_R972P 100% SAC	0.406 ± 0.007	11.30	Free flowing	4
	Ibu10_A200 25% SAC	0.372 ± 0.002	5.75	Easy flowing	3
	Ibu10_A200 50% SAC	0.421 ± 0.013	5.68	Easy flowing	3
	Ibu10_A200 75% SAC	0.420 ± 0.006	7.68	Easy flowing	3
	Ibu10_A200 100% SAC	0.422 ± 0.008	7.85	Easy flowing	3
Ibu5	uncoated	0.188 ± 0.009	0.85	Not flowing	-
	Ibu5_R972P 25% SAC	0.403 ± 0.003	6.43	Easy flowing	3
	Ibu5_R972P 50% SAC	0.403 ± 0.003	10.71	Free flowing	4
	Ibu5_R972P 75% SAC	0.401 ± 0.003	7.25	Easy flowing	3
	Ibu5_R972P 100% SAC	0.394 ± 0.002	8.33	Easy flowing	3
	Ibu5_A200 25% SAC	0.329 ± 0.004	7.84	Easy flowing	3
	Ibu5_A200 50% SAC	0.377 ± 0.004	9.03	Easy flowing	3
	Ibu5_A200 75% SAC	0.381 ± 0.002	7.94	Easy flowing	3
	Ibu5_A200 100% SAC	0.366 ± 0.011	9.57	Easy flowing	3
NB	uncoated	0.199 ± 0.003	1.63	Very cohesive	-
	FNB_R972P 25% SAC	0.378 ± 0.003	7.44	Easy flowing	2
	FNB_R972P 50% SAC	0.373 ± 0.016	17.36	Free flowing	3
	FNB_R972P 75% SAC	0.375 ± 0.003	11.26	Free flowing	3
	FNB_R972P 100% SAC	0.365 ± 0.001	10.87	Free flowing	3
	FNB_A200 25% SAC	0.353 ± 0.001	6.86	Easy flowing	2
	FNB_A200 50% SAC	0.347 ± 0.002	5.53	Easy Flowing	2
	FNB_A200 75% SAC	0.324 ± 0.002	5.07	Easy Flowing	2
	FNB A200 100% SAC	0.359 ± 0.005	9.20	Easy Flowing	2
3F	uncoated	0.287 ± 0.004	2.92	Cohesive	-
	GF_R972P 25% SAC	0.314 ± 0.006	3.20	Cohesive	0
	GF_R972P 50% SAC	0.347 ± 0.005	3.53	Cohesive	0
	GF_R972P 75% SAC	0.361 ± 0.007	3.78	Cohesive	0
	GF_R972P 100% SAC	0.361 ± 0.008	4.10	Easy flowing	1
	GF_A200 25% SAC	0.330 ± 0.007	3.12	Cohesive	0
	GF A200 50% SAC	0.340 ± 0.003	3.69	Cohesive	0
	GF_A200 75% SAC	0.340 ± 0.003 0.340 ± 0.018	3.33	Cohesive	0
	GF_A200 100% SAC	0.350 ± 0.004	4.00	Easy flowing	1



then the interparticle adhesion is given by the multi-asperity contact model that is a function of the silica SAC (14).

$$F_{vdW} = \frac{Ad}{4z_0^2} + \frac{A}{24\left(\sqrt{\left(1 + \frac{d}{D}\right)^2 - \frac{1.21d^2}{SAC*D^2}} - 1\right)^2 * D} (guest - hostcontact) \tag{6}$$

Here, A is the Hamaker constant, D is the diameter of the host particle, d is the averaged diameter of the natural asperities or the diameter of guest particles for dry coated powders, z_0 is the atomic separation distance (usually 0.4 nm) between two surfaces in contact, and SAC estimated by Eq. (1). If SAC is sufficiently high due to either the non-sparse natural asperities or adequate silica amounts, the predominant contacts are guest-guest contacts (14). For such cases, the adhesion force is independent of SAC, described by Eq. (7), shown in its full and simplified forms (14).

$$F_{ad} = \frac{A}{12z_0^2} \left[\frac{3dd}{d+d} + \frac{D}{2(L_0/z_0)^2} \right] \approx \frac{Ad}{8z_0^2} + \frac{AD}{24(2d+z_0)^2} (guset - guest contact)$$
(7)

For Eqs. (6) and (7), the Hamaker constant, A, is estimated by Eq. (8) (15,31).

$$A = 24\pi \left(\gamma_d^2\right) D_0 \tag{8}$$

In Eq. (8), γ_d is the dispersive surface energy of the original host particles or dry-coated particles, experimentally measured via IGC, and D_0 is the minimum separation distance, which is typically taken as 0.165 nm.

The Chen model depicted through Eqs. (6–8) involves several underlying assumptions such as monodisperse, spherical host and guest particles (or spherical asperities), uniform distribution of guest particles, and accurate estimation of natural asperity sizes (14). Although these assumptions could significantly limit the model's applicability, it would be worthwhile considering them based on their previously demonstrated applicability to realistic pharmaceutical powders with or without dry coating (15,28). The nano silicas used as guests satisfy some of the assumptions for dry coated powders, hence estimating the asperity size, d, is easy. However, for naturally rough particles, estimation of asperities poses a challenge. The consensus has been to specify 200 nm as an ideal asperity size (49) based on the morphology of fluidized bed cracking catalysts (FCCs), hence that may not be suitable here. An alternate approach, utilized in (15), has been proposed to estimate asperity size, $d_{\rm asp}$, as a function of the host particle size (26), Eq. (9).

$$d_{asp} = \alpha(D)^{\beta} \tag{9}$$

In the above equation, α and β are fitting parameters, and have been shown to work well for uncoated powders for $\beta = 0.6$, and $\alpha = 0.0004$ m^{0.4} (15). Further validation of Eq. (9) is necessary, although outside the scope of the

present work. Here, asperity estimates of 200 nm as well as Eq. (9) were tested.

The framework for estimating the Bo_g for all uncoated and dry coated powders using Eqs. 1, 5-9, was employed along with the data from Tables III, IV, and V as well as the IGC-based dispersive surface energy measurements for all dry coated powders. Three different versions for estimating the asperities for uncoated powders were considered and depicted in Fig. 4 for the computation of Bo_o. Figures 4(a) and 4(b), were based on a fixed asperity size of 200 nm or variable asperity sizes from Eq. (9), respectively. In both those cases, the rank-ordering of the Bo_g values for various uncoated APIs (Ibu20 < Ibu10 < GF < FNB < Ibu5) did not match well with the rank-ordering of bulk properties such as the FFC (Ibu20 < GF < FNB < Ibu10 < Ibu5) and BD (GF < Ibu20 < Ibu10 < FNB < Ibu5). In addition, the Bo_g reductions after dry coating were not in line with the corresponding enhancements in the FFC and BD. For example, the enhancements in the bulk properties after dry coating for GF were the lowest as compared to all other APIs, whereas the reductions in Bo_{σ} after dry coating were not the lowest, see Figs. 4(a) and 4(b). In contrast, examination of Fig. 4(c) revealed that the uncoated API Bo_{σ} (GF < Ibu20 < Ibu10 < FNB < Ibu5) better followed the rank-ordering of the measured FFC (Ibu20 < GF < FNB < Ibu10 < Ibu5) and bulk densities (GF < Ibu20 < Ibu10 < FNB < Ibu5). Most importantly, the lowest levels of enhancements in FFC and BD after dry coating for GF were better captured in Bo_{α} estimated in Fig. 4(c). In addition, the higher macro-scale surface roughness of GF was most likely responsible for the underestimation of the amount of silica required at various theoretical SAC % values, potentially another source of inaccurate estimation in the Bo_g reduction. Overall, the accurate estimation of the surface roughness of uncoated pharmaceutical powders would be a future topic worth further investigation to enable accurate estimation of Bo_{o} , which is an important particle scale measure.

As seen in Fig. 4(c), dry coating using either silica led to the reduction in Bo_g , where maximum reductions ranged from one to over two orders of magnitude. The order of greatest to lowest reduction was Ibu20 > Ibu5 > Ibu10 > F NB > GF; the lowest in GF was corroborated by its insufficient reduction in the FFC and BD values. As expected, there were variations within each API in terms of relative enhancements driven both by the silica type and the SAC % of silica. Regardless, such dramatic decreases in their Bo_g were behind their corresponding flow regime improvements (Table V and Fig. 3(a)), enhanced BD values (Fig. 3(b)), and the corresponding reduction in AR (Fig. 2).

As a novelty of this paper, the reduced agglomeration emerged as the single most interesting, relevant, yet often overlooked despite being an obvious measure, because of the ease of testing requiring very small quantities of the



Fig. 4 Granular Bond number values before and after dry coating at varying % SAC for each API. For dry coated powders, guest- guest contact (Eq. 7) for R972P of 50 SAC% and for A200 of 75 SAC % and greater.

(a) Uncoated API asperities assumed to be 200 nm.

(b) Uncoated API asperities estimated through Eq. (9). (c) Uncoated API asperities taken as 1 nm for FNB and all Ibu cases, and 500 nm for GF

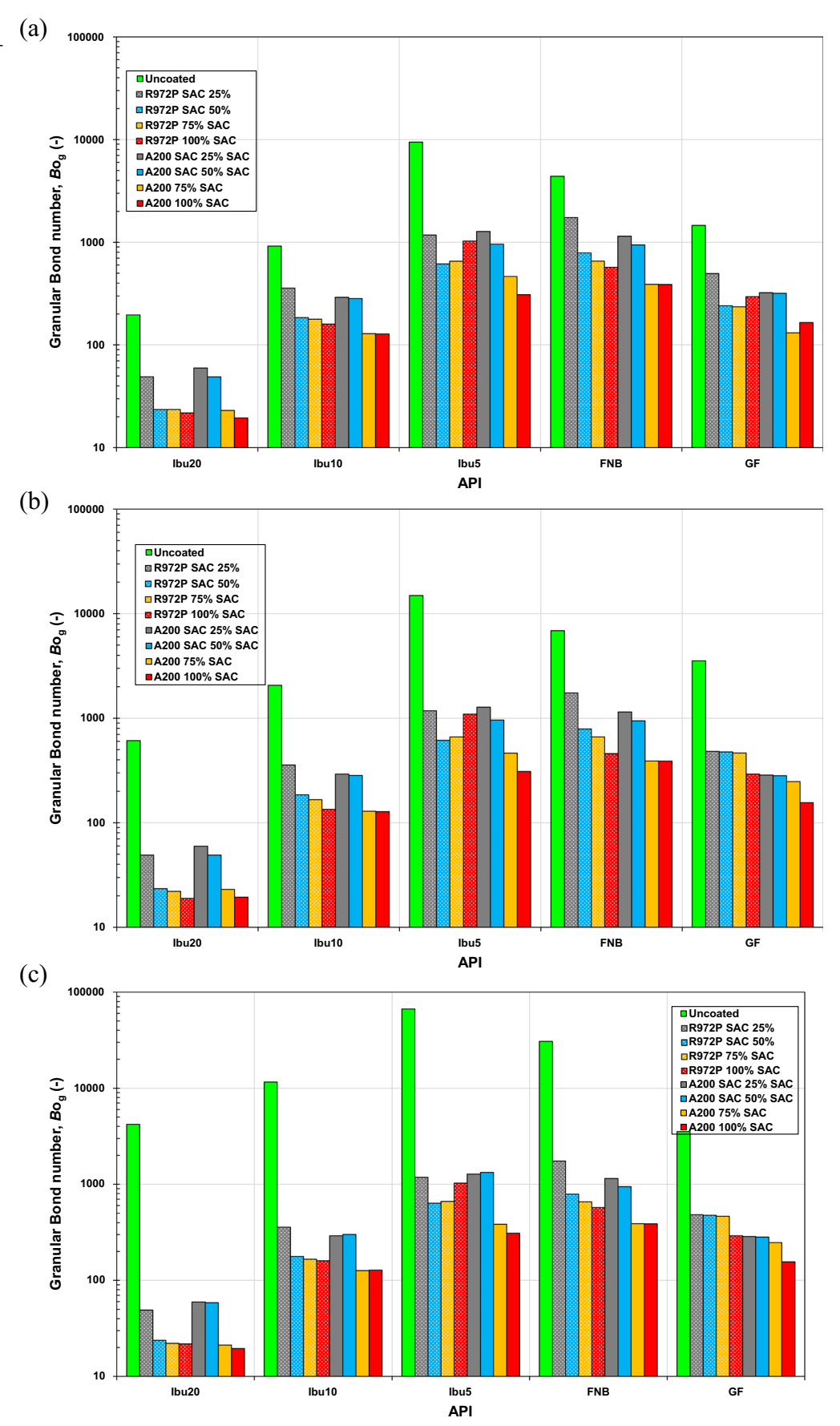
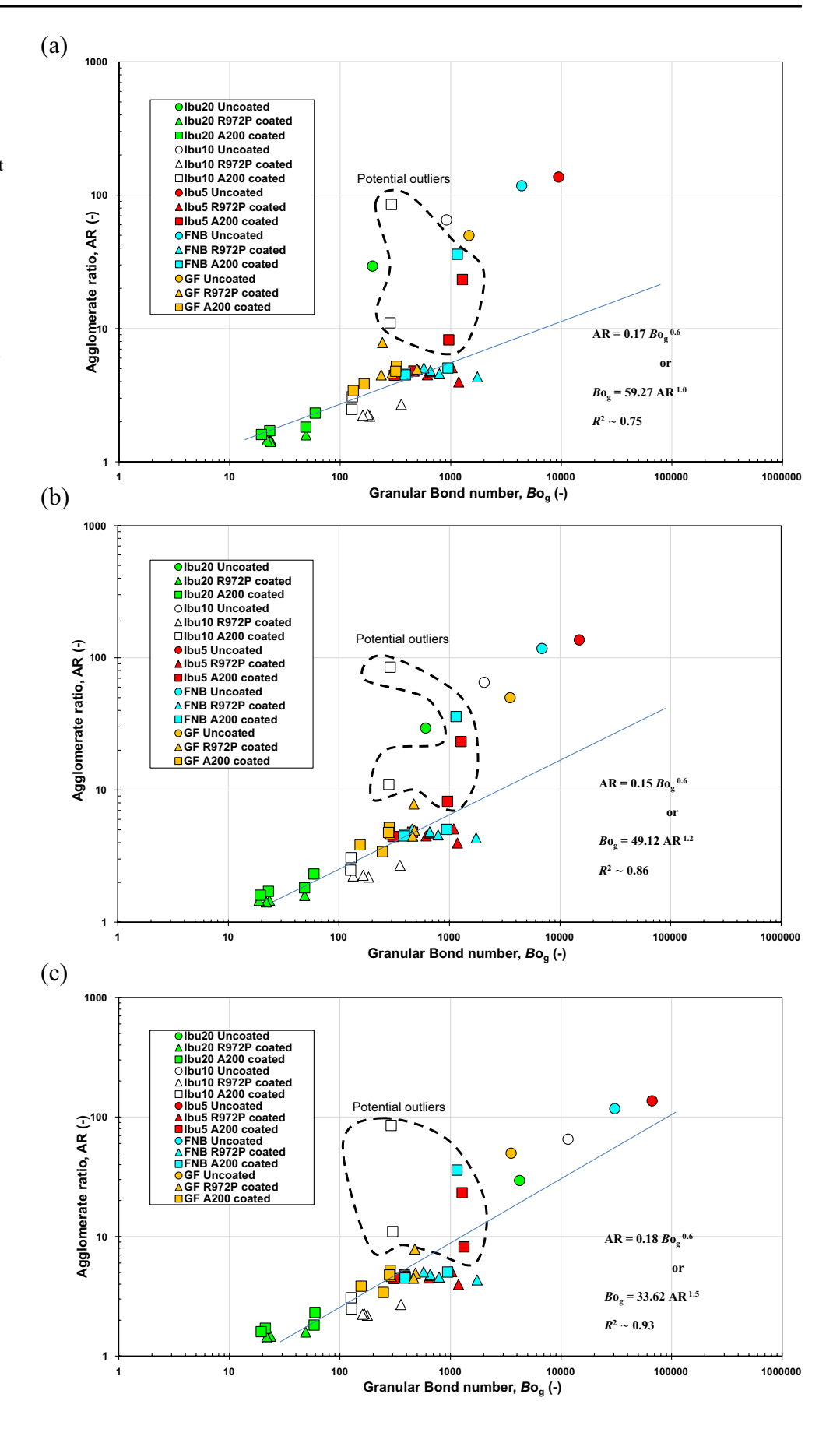




Fig. 5 The agglomerate ratio (AR) plotted as a function of granular Bond number, Bo_{σ} . For dry coated powders, guest- guest contact (Eq. 7) for R972P SAC \geq 50%, for A200 SAC \geq 75%. Best fitted lines not including five apparent outliers. (a) Uncoated API asperities assumed to be 200 nm. (b) Uncoated API asperities estimated through Eq. (9). (c) Uncoated API asperities taken as 1 nm for FNB and all Ibu cases, and 500 nm for GF. The power law relationship between AR and Bog was the most evident for case (c), further supporting the need for more reliable estimation of natural surface roughness and corresponding asperity sizes.



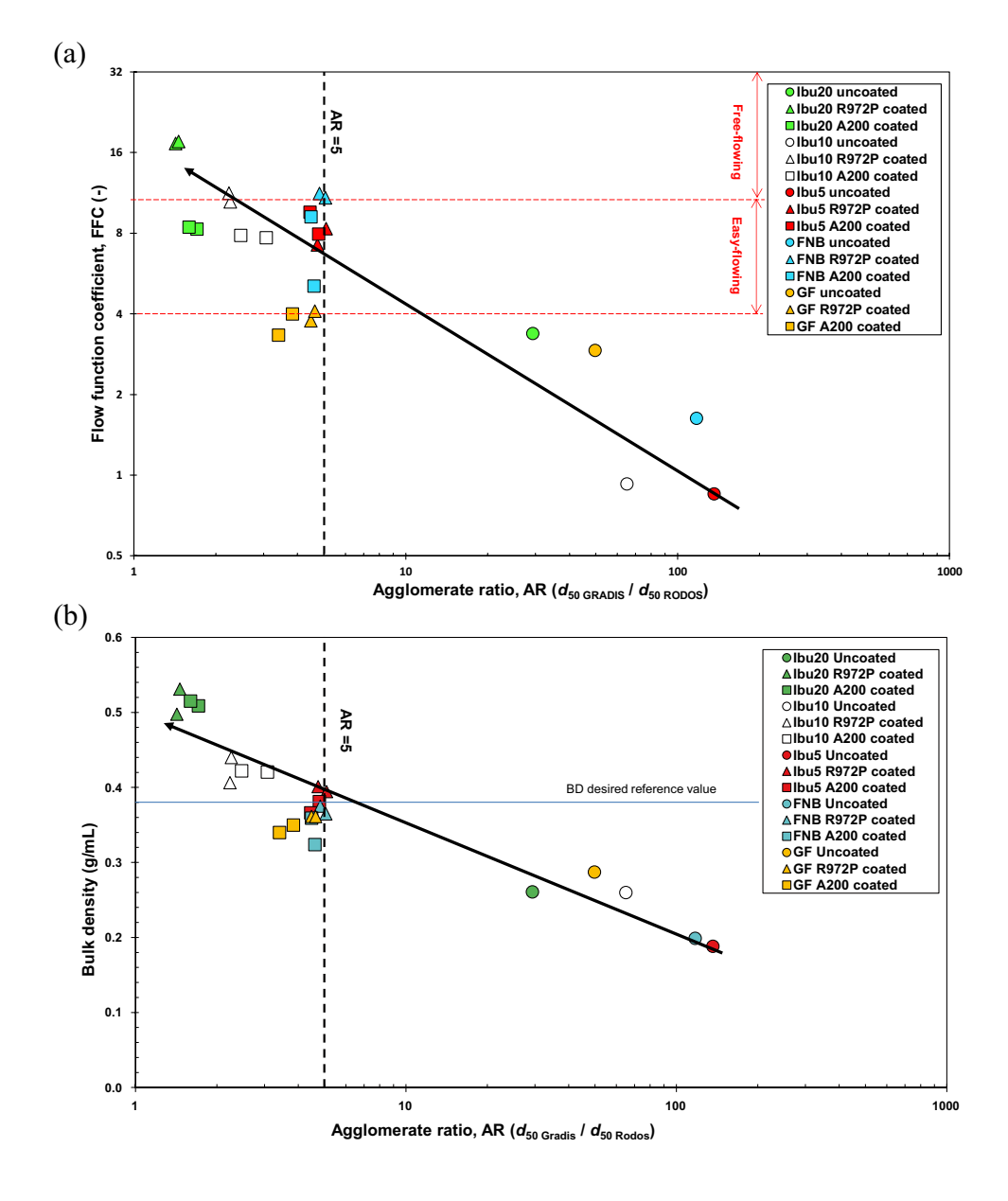


powders using the generally available particle sizing instruments. Another advantage of considering agglomeration as a critical attribute of fine powders is the established powerlaw relationship between the Bo_g and AR values (12,50–52). Such relationship was examined for these powders through log-log plots of AR values as functions of Bo_g in Figs. 5(a) through 5(c), each figure corresponding to the assumed uncoated powder surface asperity values used for Figs. 4(a) through 4(c). For each case, power-law relation was tested for all the data points, excluding five possible outliers that were identified as having unexpected and unexplainable high levels of agglomeration. The expected power-law trend was the most suitable and evident in Fig. 5(c), further supporting the need for the proper estimation of natural surface roughness values. Identifying such a relationship through a careful experimental investigation would facilitate approximate estimation of the magnitude of $Bo_{\rm g}$ in the future, done through just assessing the AR of uncoated and dry coated powders. Such ability would also enable preliminary, first order prediction of the related bulk properties such as the FFC or BD, discussed next.

Flowability (FFC) and Bulk Density (BD) as Functions of Agglomerate Ratio (AR)

As discussed above, accurate estimation of the Bo_g would not be easy for typical pharmaceutical powders, making the prediction of bulk properties from particle scale properties even more challenging (28). In the light of the relationship between agglomeration, which is a small-ensemble bulk-scale measure, with particle-scale measure (Bo_g , Fig. 5(c)),

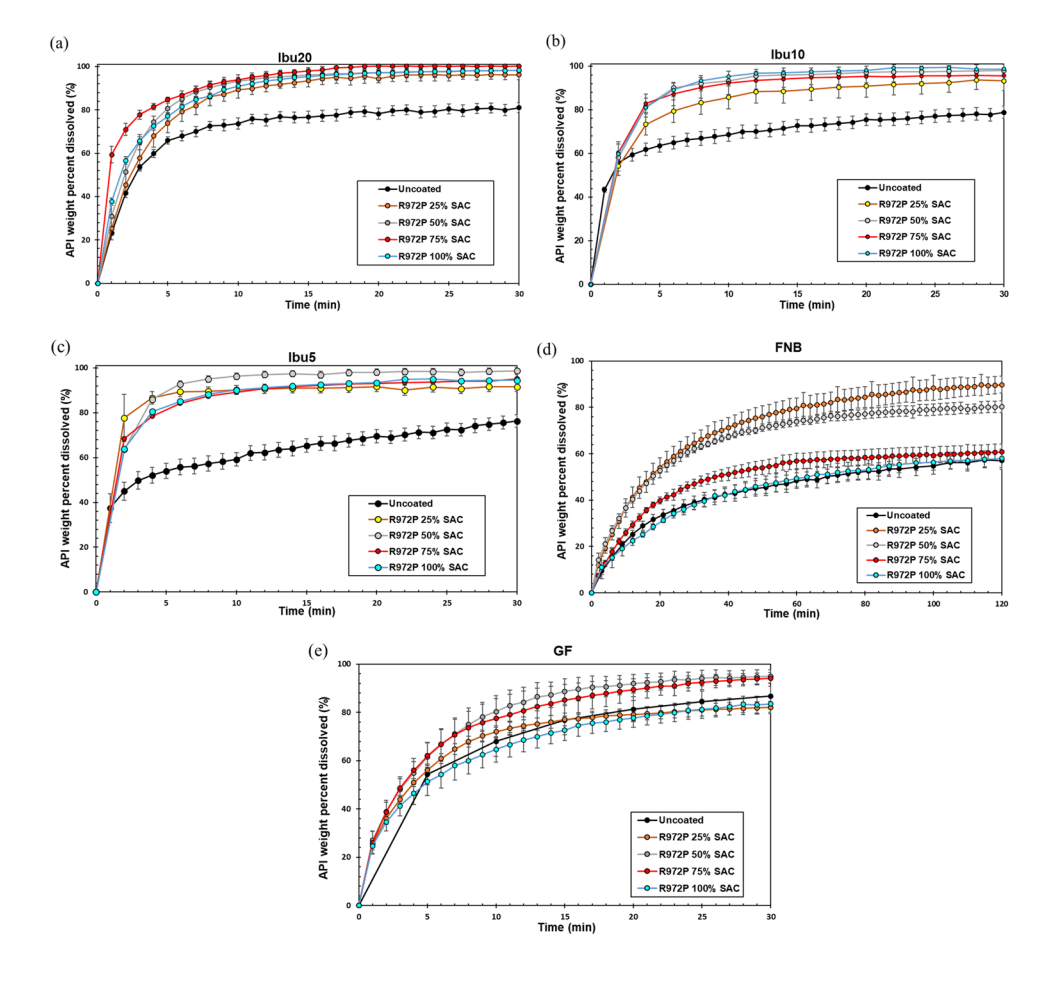
Fig. 6 Bulk powder properties as functions of Agglomerate Ratio (AR) for uncoated and dry coated (75 and 100% SACs) APIs. (a) Powder flowability (FFC); (b) bulk density (BD); horizontal reference line for the desirable BD level for direct compression tableting. Illustrative freehand lines intended to depict the general trend of FFC and BD.





the relationship between AR and bulk properties such as FFC and BD were considered. However, based on the relatively lower SAC levels for the apparent outliers even for Fig. 5(c), it was evident that for dry coated APIs, lower SAC level (25 and 50%) cases would generally underperform. Accordingly, FFC values (log base 2) for all uncoated and dry coated (75 and 100% SACs) APIs were plotted as functions of AR (log base 10), Fig. 6(a). While there was scatter even without considering the lower SAC levels (25 and 50%), a reasonable trend of increased FFC with decreasing AR could be observed. In fact, for AR of five or lower, the FFC values were within easy flowing or free flowing regimes. As expected, GF underperformed. BD as a function or AR (log base 10) shown in Fig. 6(b) exhibited much less scatter, and for AR of five or lower, the BD values were equal to or above the reference line that suggest amenability for direct compression tableting. These results demonstrated that uncoated fine powders had higher AR values and poorer FFC and BD values, whereas significantly reduced AR values due to dry coating were indicative of improved FFC and BD. In summary, assessment of AR of fine powders could provide a quick indication of their bulk properties and the extent of FFC and BD enhancement with dry coating, just based on the extent of reduction in AR.

Fig. 7 Dissolution profiles of the uncoated as well as hydrophobic silica (R972P) coated APIs. (a) Ibu20; (b) Ibu10; (c) Ibu5; (d) FNB; and (e) GF. The time range was 30 min, except for FNB that was 120 min to assure at least 60% API was dissolved; these profiles with the specified time range were used to calculate the area under the dissolution curve, AUC.



Dissolution

Dissolution profiles were obtained using the USP IV method in all five cases of uncoated and dry coated APIs for assessing the impact of type and amounts of silica. The most interesting outcome, although counterintuitive, was that the dissolution performance improved even with hydrophobic silica (R972P) coating for all five APIs, as shown in Figs. 7(a) through 7(e). The surface wettability of all cases of uncoated and dry coated APIs was assessed following the methods discussed in Sect. 2.2.9, see Table VI, confirming that the R972P coated APIs were indeed more hydrophobic as indicated by their increased contact angle values. Regardless, the enhancements for Ibu20, Ibu10, and Ibu5 were significant at all levels of R972P % SAC. For FNB, the dissolution enhancement was highest at 25% SAC, closely followed by 50% SAC, indicating a diminishing effect beyond a certain amount of silica. For GF, the dissolution enhancement was highest at 50% SAC, closely followed by 75% SAC, but for 25 and 100% SAC, there was no enhancement. The dissolution results for Ibu and GF agreed with the previous work (22,53), which employed de-ionized water as the dissolution medium, whereas the current work employed a 12 mM SDS aqueous solution to ensure adequate solubility for all APIs,

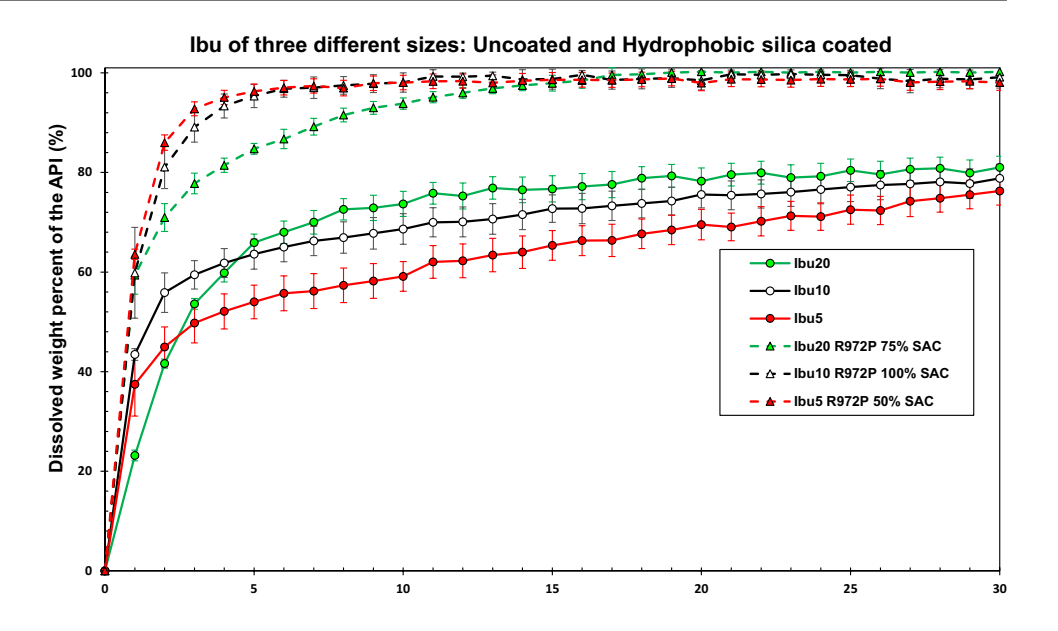


Table VI Surface Wettability Test Outcomes, Dissolution AUC, and Normalized AUC. For Uncoated API, AUC is Noted in Red

API	Sample ID	Packing factor C (m ⁵)	Surface contact angle (°)	AUC evaluation time range (min)	Area under the dissolution curve, AUC (%*sec)	Normalized AUC with respect to time AUC/time (%)
Ibu20	Uncoated Ibu20	8.54×10^{-14}	73	30	2133	1.19
	Ibu20-R972P-25SAC	4.07×10^{-16}	73		2539	1.41
	Ibu20-R972P-50SAC	8.14×10^{-16}	74		2641	1.47
	Ibu20-R972P-75SAC	1.22×10^{-15}	76		2761	1.53
	Ibu20-R972P-100SAC	1.63×10^{-15}	81		2624	1.46
	Ibu20-A200-25SAC	2.20×10^{-16}	72		2621	1.46
	Ibu20-A200-50SAC	4.07×10^{-16}	70		2559	1.42
	Ibu20-A200-75SAC	4.27×10^{-16}	72		2461	1.37
	Ibu20-A200-100SAC	4.19×10^{-16}	68		2721	1.51
Ibu10	Uncoated Ibu10	2.93×10^{-16}	73		1875	1.04
	Ibu10-R972P-25SAC	2.01×10^{-15}	75		2480	1.38
	Ibu10-R972P-50SAC	3.26×10^{-15}	79		2365	1.31
	Ibu10-R972P-75SAC	4.33×10^{-15}	84		2344	1.30
	Ibu10-R972P-100SAC	1.14×10^{-14}	87		2382	1.32
	Ibu10-A200-25SAC	1.73×10^{-15}	70		2513	1.40
	Ibu10-A200-50SAC	2.79×10^{-15}	71		2600	1.44
	Ibu10-A200-75SAC	4.18×10^{-15}	70		2728	1.52
	Ibu10-A200-100SAC	5.42×10^{-15}	68		2696	1.50
Ibu5	Uncoated Ibu5	4.27×10^{-16}	70		1619	0.90
1005	Ibu5-R972P-25SAC	1.34×10^{-15}	72		2597	1.44
	Ibu5-R972P-50SAC	2.73×10^{-15}	72		2727	1.51
	Ibu5-R972P-75SAC	2.73×10^{-15}	79		2582	1.43
	Ibu5-R972P-100SAC	3.63×10^{-15}	84		2592	1.44
	Ibu5-A200-25SAC	7.16×10^{-16}	70		2163	1.20
	Ibu5-A200-50SAC	2.44×10^{-15}	68		2405	1.34
	Ibu5-A200-75SAC	1.00×10^{-15}	67		2587	1.44
	Ibu5-A200-100SAC	1.93×10^{-15}	67		2710	1.51
FNB	Uncoated FNB	2.17×10^{-14}	73	120	5295	0.74
FIND		1.86×10^{-15}		120		
	FNB-R972P-25SAC	2.67×10^{-15}	83		8621	1.20
	FNB-R972P-50SAC	2.51×10^{-15}	83		7996	1.11
	FNB-R972P-75SAC	2.81×10^{-15}	84		6030	0.84
	FNB-R972P-100SAC		84		6069	0.84
	FNB-A200-25SAC	1.13×10^{-15}	70		8067	1.12
	FNB-A200-50SAC	1.31×10^{-15}	70		8435	1.17
	FNB-A200-75SAC	1.55×10^{-15}	69		8293	1.15
a =	FNB-A200-100SAC	1.64×10^{-15}	65	•	8931	1.24
GF	Uncoated GF	8.14×10^{-17}	70	30	2041	1.13
	GF-R972P-25SAC	1.22×10^{-16}	71		2084	1.16
	GF-R972P-50SAC	2.03×10^{-16}	81		2376	1.32
	GF-R972P-75SAC	8.14×10^{-16}	87		2322	1.29
	GF-R972P-100SAC	1.22×10^{-15}	87		2000	1.11
	GF-A200-25SAC	1.63×10^{-16}	70		2468	1.37
	GF-A200-50SAC	2.03×10^{-16}	69		2406	1.34
	GF-A200-75SAC	8.14×10^{-16}	68		2490	1.38
	GF-A200-100SAC	4.07×10^{-16}	67		2579	1.43



Fig. 8 Dissolution profiles for three different particle sizes of Ibu, uncoated or dry coated with hydrophobic silica; % SAC selected for each case that resulted in the highest dissolution performance during 30 min of dissolution.



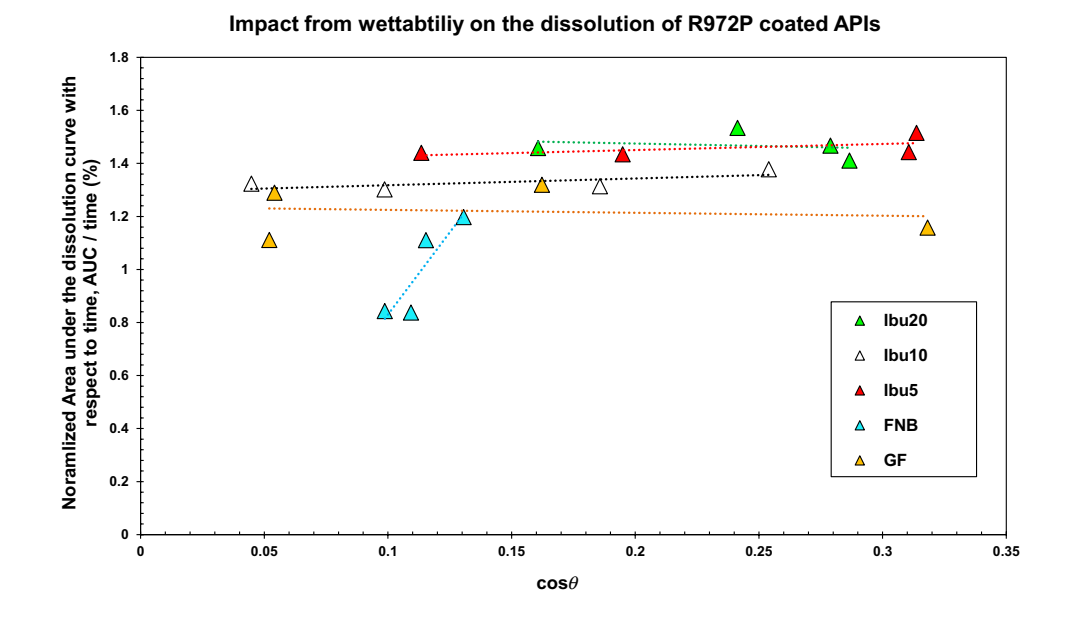
including FNB, which could not be fully dissolved in de-ionized water (33). As expected, the dissolution enhancements due to hydrophilic silica (A200) coating were significant in all cases and a usually higher level of silica led to better performance, shown in Figure S2, *Supplementary Materials*.

Dissolution profiles for Ibu20, Ibu10 and Ibu5 before and after R972P dry coating revealed very interesting patterns, see Fig. 8. These outcomes, substantiating previous reports, demonstrate that for uncoated Ibu, as the particle size decreased, the dissolution rate deteriorated instead of improving due to the particle size reduction and a corresponding increase in available surface area. This known phenomenon was attributed to the agglomeration of milled or micronized powders (18). In contrast, after dry coating with even hydrophobic silica (R972P), greatly reduced

agglomeration counteracts the increased hydrophobicity (increased contact angle, Table VI). Consequently, the maximum achieved dissolution performance for Ibu20, Ibu10, and Ibu5 followed the expected trend of increase as the sizes were reduced and the available surface area increased, supporting, and further validating previously reported trends (22).

Dry coating with the hydrophilic silica (A200) leads to two complementary positive impacts, agglomerate size reduction (Fig. 2) and reduced wetting angle (Table VI), on poorly water-soluble drug dissolution. A more interesting case was the hydrophobic silica (R972P) for which these effects are conflicting and the competition between the two dictated the outcome. Whereas dry coating with R972P led to increased wetting angle (Table VI), the

Fig. 9 Dissolution rate evaluated for all R972P coated APIs with respect to the surface wettability. Area under the dissolution curve for each API was normalized with respect to the time since they varied in time where they reached minimum of 60% dissolved.





greatly reduced agglomeration (Fig. 2) outweighed that negative effect for most cases except for the highest level of R972P silica. Such behavior was captured in Fig. 9, for all five R972P coated APIs for the dissolution area under the curve (AUC) as a function of the cosine of the wetting angle. Ideally, for such comparison, the dissolution rate kinetic analysis would be required for each API/silica combination. However, for the agglomerates, standard dissolution kinetics models (54–56) would not be applicable. Therefore, the AUC for time duration for which a minimum of 60% of the original % weight of API was dissolved had to be evaluated and used (54-56). The time taken for FNB was four times that of other APIs. Hence, the AUC was normalized with respect to time (Table VI), which is 30 min for all APIs except FNB, which is 120 min due to its significantly lesser solubility. For Ibu20, Ibu10, Ibu5, and GF, the normalized AUC was essentially unchanged as a function of wettability, implying the dissolution was driven by the reduced agglomeration.

For FNB, however, both the wettability and agglomeration reduction impacts were evident in the trend, as the two lowest normalized AUC values were for 75 and 100% SAC of R972P, and the highest level was for 25% SAC of R972P. Such outcomes were reasonable, considering the lowest water solubility and highest LogP of FNB (Table I). Nonetheless, even for FNB, the agglomerate reduction impact was significant as evident from the dissolution profiles in Fig. 7(d) because all cases expect 100% SAC of R972P outperformed uncoated FNB, which has a lower wetting angle than all R972P coated cases (Table VI).

In summary, dissolution of coated micronized APIs was enhanced even when the hydrophobic silica R972P was used, confirming the significant impact of reduced agglomeration after dry coating. Whereas the hydrophilic silica such as A200 would be an obvious choice for poorly water-soluble APIs from the perspective of enhanced dissolution, using a judiciously selected amount of hydrophobic silica such as R972P would be a more desirable option, due to its benefits such as higher agglomerate reduction, better flowability and enhanced bulk density.

CONCLUSION

This work demonstrated the prominent role played by reduced agglomeration after dry coating with silica, including hydrophobic R972P, hence potentially removing the taboo against its use, on the enhanced dissolution of fine poorly water-soluble APIs. Several other important findings include: (1) For all five different APIs/sizes, dry coating led to enhanced processability through up to four flow regime enhancement, up to 100% increase in BD, and 1–2 orders of magnitude reduction in agglomeration leading to dissolution AUC enhancement up to 60%. (2) As a major novelty,

agglomeration (AR), quicker material sparing measure, was a key indicator of both processability and dissolution of fine APIs. (3) The AR- Bo_g exhibit power-law relationship for fine APIs, removing the explicit need for assessing Bo_g . (4) AR was well-correlated with both FFC and BD, greatly facilitating the determination of dry coating efficacy for processability enhancement and setting AR \leq 5 as a bar for powder processability. (5) The natural surface roughness of the uncoated particles has a major role on bulk properties, hence its proper estimation is necessary; using 200 nm (or size based estimation (26)) may not be appropriate. (6) For APIs such as ibuprofen, milling would significantly increase surface energy values, further increasing effective powder cohesion, requiring dry coating-based passivation (11,21).

Supplementary Information The online version contains supplementary material available at https://doi.org/10.1007/s11095-022-03293-z.

ACKNOWLEDGMENTS AND DISCLOSURES The authors thank Hira Khurshid for her assistance in sample preparation and testing from, and Roopal Bhat, Christopher Kossor, and Siddharth Tripathi for their editorial input. The authors have no conflicts of interest or sources of competing interest to declare. Partial support for this work from IFPRI is gratefully acknowledged.

References

- Lipinski C. Poor aqueous solubility An industry wide problem in drug discovery. American Pharmaceutical Review. 2002;5(3):82-5.
- Kalepu S, Nekkanti V. Insoluble drug delivery strategies: Review of recent advances and business prospects. Acta Pharmaceutica Sinica B. 2015;5(5):442–53.
- Hu J, Rogers TL, Brown J, Young T, Johnston KP, Williams Iii RO. Improvement of dissolution rates of poorly water soluble APIs using novel spray freezing into liquid technology. Pharm Res. 2002;19(9):1278–84.
- Han X, Ghoroi C, To D, Chen Y, Davé R. Simultaneous micronization and surface modification for improvement of flow and dissolution of drug particles. Int J Pharm. 2011;415(1–2):185–95.
- da Costa MA, Seiceira RC, Rodrigues CR, Hoffmeister CRD, Cabral LM, Rocha HVA. Efavirenz dissolution enhancement I: Co-micronization. Pharmaceutics. 2013;5(1):1–22.
- Bhakay A, Azad M, Bilgili E, Dave R. Redispersible fast dissolving nanocomposite microparticles of poorly water-soluble drugs. Int J Pharm. 2014;461(1–2):367–79.
- Krull SM, Susarla R, Afolabi A, Li M, Ying Y, Iqbal Z, Bilgili E, Davé RN. Polymer strip films as a robust, surfactant-free platform for delivery of BCS Class II drug nanoparticles. Int J Pharm. 2015;489(1–2):45–57.
- Nase ST, Vargas WL, Abatan AA, McCarthy JJ. Discrete characterization tools for cohesive granular material. Powder Technol. 2001;116(2–3):214–23.
- Harnby N. The mixing of cohesive powders. In: Neinow AW, Edwards, M.F., Harnby, N., editor. Mixing in the Process Industries: Second edition Butterworth-Heinemann; 1992. p. 79–96.
- Feng JQ, Hays DA. Relative importance of electrostatic forces on powder particles. Powder Technol. 2003;135–136:65–75.



- Han X, Jallo L, To D, Ghoroi C, Davé R. Passivation of highsurface-energy sites of milled ibuprofen crystals via dry coating for reduced cohesion and improved flowability. J Pharm Sci. 2013;102(7):2282–96.
- Castellanos A. The relationship between attractive interparticle forces and bulk behaviour in dry and uncharged fine powders. Adv Phys. 2005;54(4):263–376.
- 13. Yang J, Sliva A, Banerjee A, Dave RN, Pfeffer R. Dry particle coating for improving the flowability of cohesive powders. Powder Technol. 2005;158(1–3):21–33.
- Chen Y, Yang J, Dave RN, Pfeffer R. Fluidization of coated group C powders. AIChE J. 2008;54(1):104–21.
- Capece M, Huang Z, To D, Aloia M, Muchira C, Davé RN, Yu AB. Prediction of porosity from particle scale interactions: Surface modification of fine cohesive powders. Powder Technol. 2014;254:103–13.
- Jallo LJ, Ghoroi C, Gurumurthy L, Patel U, Davé RN. Improvement of flow and bulk density of pharmaceutical powders using surface modification. Int J Pharm. 2012;423(2):213–25.
- Huang Z, Scicolone JV, Gurumuthy L, Davé RN. Flow and bulk density enhancements of pharmaceutical powders using a conical screen mill: A continuous dry coating device. Chem Eng Sci. 2015;125:209–24.
- De Villiers MM. Influence of agglomeration of cohesive particles on the dissolution behaviour of furosemide powder. Int J Pharm. 1996;136(1–2):175–9.
- Huang Z, Xiong W, Kunnath K, Bhaumik S, Davé RN. Improving blend content uniformity via dry particle coating of micronized drug powders. Eur J Pharm Sci. 2017;104:344–55.
- Kim S, C. Castillo, M. Sayedahmed, Dave RN. Reduced fine API agglomeration after dry coating for enhanced blend uniformity and processability of low drug loaded blends Pharmaceutical Research. 2022;under review.
- Han X, Ghoroi C, Davé R. Dry coating of micronized API powders for improved dissolution of directly compacted tablets with high drug loading. Int J Pharm. 2013;442(1–2):74–85.
- Kim S, Bilgili E, Davé RN. Impact of altered hydrophobicity and reduced agglomeration on dissolution of micronized poorly water-soluble drug powders after dry coating. International Journal of Pharmaceutics. 2021;606.
- Chen L, Liu J, Zhang Y, Zhang G, Kang Y, Chen A, Feng X, Shao L. The toxicity of silica nanoparticles to the immune system. Nanomedicine. 2018;13(15):1939–62.
- Kunnath K, Huang Z, Chen L, Zheng K, Davé R. Improved properties of fine active pharmaceutical ingredient powder blends and tablets at high drug loading via dry particle coating. Int J Pharm. 2018;543(1-2):288-99.
- 25. McCarthy JJ, Khakhar DV, Ottino JM. Computational studies of granular mixing. Powder Technol. 2000;109(1–3):72–82.
- 26. Yu AB, Feng CL, Zou RP, Yang RY. On the relationship between porosity and interparticle forces. Powder Technol. 2003;130(1-3):70-6.
- 27. Chen Y, Jallo L, Quintanilla MAS, Dave R. Characterization of particle and bulk level cohesion reduction of surface modified fine aluminum powders. Colloids Surf, A. 2010;361(1-3):66-80.
- Kunnath K, Chen L, Zheng K, Davé RN. Assessing predictability of packing porosity and bulk density enhancements after dry coating of pharmaceutical powders. Powder Technol. 2021;377:709–22.
- Rumpf H. Die Wissenschaft des Agglomerierens. Chem Ing Tec. 1974;46(1):1.
- Rabinovich YI, Adler JJ, Ata A, Singh RK, Moudgil BM. Adhesion between nanoscale rough surfaces. I. Role of asperity geometry. Journal of Colloid and Interface Science. 2000;232(1):10–16.

- Chen Y, Quintanilla MAS, Yang J, Valverde JM, Dave RN. Pulloff force of coated fine powders under small consolidation. Physical Review E Statistical, Nonlinear, and Soft Matter Physics.
 2009:79(4).
- Jallo LJ, Chen Y, Bowen J, Etzler F, Dave R. Prediction of interparticle adhesion force from surface energy and surface roughness. J Adhes Sci Technol. 2011;25(4–5):367–84.
- 33. Azad M, Afolabi A, Bhakay A, Leonardi J, Davé R, Bilgili E. Enhanced physical stabilization of fenofibrate nanosuspensions via wet co-milling with a superdisintegrant and an adsorbing polymer. Eur J Pharm Biopharm. 2015;94:372–85.
- Freeman R. Measuring the flow properties of consolidated, conditioned and aerated powders A comparative study using a powder rheometer and a rotational shear cell. Powder Technol. 2007;174(1-2):25-33.
- Schulze D, Schwedes J, Carson JW. Powders and bulk solids: Behavior, characterization, storage and flow; 2008.
- Chen L, Ding X, He Z, Fan S, Kunnath KT, Zheng K, Davé RN. Surface engineered excipients: II. Simultaneous milling and dry coating for preparation of fine-grade microcrystalline cellulose with enhanced properties. International Journal of Pharmaceutics. 2018;546(1–2):125–136.
- Jallo LJ, Dave RN. Explaining Electrostatic Charging and Flow of Surface-Modified Acetaminophen Powders as a Function of Relative Humidity Through Surface Energetics. J Pharm Sci. 2015;104(7):2225–32.
- 38. Wu S. Polar and nonpolar interactions in adhesion. J Adhes. 1973;5(1):39–55.
- 39. Barra J, Lescure F, Falson-Rieg F, Doelker E. Can the organization of a binary mix be predicted from the surface energy, cohesion parameter and particle size of its components? Pharm Res. 1998;15(11):1727–36.
- Zheng K, Kunnath K, Ling Z, Chen L, Davé RN. Influence of guest and host particle sizes on dry coating effectiveness: When not to use high mixing intensity. Powder Technol. 2020;366:150–63.
- 41. Alway B, Sangchantra R, Stewart PJ. Modelling the dissolution of diazepam in lactose interactive mixtures. Int J Pharm. 1996;130(2):213–24.
- 42. Chander S, Hogg R, Fuerstenau DW. Characterization of the wetting and dewetting behavior of powders. Kona Powder Part J. 2007;25(March):56–75.
- 43. Washburn EW. The dynamics of capillary flow. Phys Rev. 1921;17(3):273–83.
- Thakker M, Karde V, Shah DO, Shukla P, Ghoroi C. Wettability measurement apparatus for porous material using the modified Washburn method. Measurement Science and Technology. 2013;24(12).
- Sievens-Figueroa L, Pandya N, Bhakay A, Keyvan G, Michniak-Kohn B, Bilgili E, Davé RN. Using USP i and USP IV for discriminating dissolution rates of nano- and microparticle-loaded pharmaceutical strip-films. AAPS PharmSciTech. 2012;13(4):1473–82.
- 46. Bolten D, Lietzow R, Türk M. Solubility of ibuprofen, phytosterol, salicylic acid, and naproxen in aqueous solutions. Chem Eng Technol. 2013;36(3):426–34.
- Rao VM, Lin M, Larive CK, Southard MZ. A mechanistic study of griseofulvin dissolution into surfactant solutions under laminar flow conditions. J Pharm Sci. 1997;86(10):1132–7.
- 48. Chattoraj S, Shi L, Sun CC. Profoundly improving flow properties of a cohesive cellulose powder by surface coating with nano-silica through comilling. J Pharm Sci. 2011;100(11):4943–52.
- Massimilla L, Donsi G. Cohesive forces between particles of fluidbed catalysts. Powder Technol. 1976;15(2):253–60.
- Witten TA, Sander LM. Diffusion-limited aggregation, a kinetic critical phenomenon. Phys Rev Lett. 1981;47(19):1400–3.



- 51. Matsoukas T, Friedlander SK. Dynamics of aerosol agglomerate formation. Journal of Colloid And Interface Science. 1991;146(2):495–506.
- Wu MK, Friedlander SK. Note on the power law equation for fractal-like aerosol agglomerates. Journal of Colloid And Interface Science. 1993;159(1):246–8.
- Qu L, Zhou Q, Denman JA, Stewart PJ, Hapgood KP, Morton DAV. Influence of coating material on the flowability and dissolution of dry-coated fine ibuprofen powders. Eur J Pharm Sci. 2015;78:264–72.
- 54. Peppas NA. Analysis of Fickian and non-Fickian drug release from polymers. Pharm Acta Helv. 1985;60(4):110–1.
- Ritger PL, Peppas NA. A simple equation for description of solute release I. Fickian and non-fickian release from non-swellable devices in the form of slabs, spheres, cylinders or discs. Journal of Controlled Release. 1987;5(1):23–36.
- Peppas NA, Sahlin JJ. A simple equation for the description of solute release. III. Coupling of diffusion and relaxation. International Journal of Pharmaceutics. 1989;57(2):169–172.

Publisher's Note Springer Nature remains neutral with regard to jurisdictional claims in published maps and institutional affiliations.

